

Simple Baselines for Human Pose Estimation and Tracking

Bin Xiao^{1*}, Haiping Wu^{2*†}, and Yichen Wei¹

¹Microsoft Research Asia, ²University of Electronic Science and Technology of China
 {Bin.Xiao, v-haipwu, yichenw}@microsoft.com

Abstract. There has been significant progress on pose estimation and increasing interests on pose tracking in recent years. At the same time, the overall algorithm and system complexity increases as well, making the algorithm analysis and evaluation more difficult. This work provides baseline methods that are surprisingly simple and effective, thus helpful for inspiring and evaluating new ideas for the field. State-of-the-art results are achieved on challenging benchmarks. The code will be released.

Keywords: Pose Estimation, Pose Tracking

1 Introduction

Similar as many vision tasks, the progress on human pose estimation problem is significantly advanced by deep learning. Since the pioneer work in [1,2], the performance on the MPII benchmark [3] has become saturated quickly, starting from about 80% PCKH@0.5 [2] to more than 90% [4,5,6,7,8] in three years. The progress on the more recent and challenging COCO human pose benchmark [9] is even faster. The mAP metric is increased from 60.5 (COCO 2016 Challenge winner [10,11]) to 72.1 (COCO 2017 Challenge winner [12,10]) in one year. With the quick maturity of pose estimation, a more challenging task of “simultaneous pose detection and tracking in the wild” has been introduced recently [13].

At the same time, the network architecture and experimental practice have steadily become more complex. This makes the algorithm analysis and evaluation more difficult. For example, the leading methods [4,5,6,7,8] on MPII benchmark [3] have considerable difference in many details but minor difference in accuracy. It is hard to tell which details are crucial. Also, the representative works [14,15,16,12,11] on COCO benchmark are also complex but differ significantly. Comparison between such works is mostly on system level and less informative. About pose tracking, although there has not been much work [17], the system complexity can be expected to further increase due to the increased problem dimension and solution space.

This work aims to ease this problem by asking a question from the opposite direction, *how good could a simple method be?* To answer the question, this

*Equal contribution.

†This work is done when Haiping Wu is an intern at Microsoft Research Asia.

work provides baseline methods for both pose estimation and tracking. They are surprisingly simple and effective. Thus, they hopefully would help inspiring new ideas and simplifying their evaluation. The code, as well as pre-trained models, will be released to facilitate the research community.

Pose estimation is based on a few deconvolutional layers added on a backbone network, ResNet [18] in this work. It is probably the simplest way to estimate heat maps from deep and low resolution features. Our *single* model’s best result achieves the state-of-the-art at mAP of 73.8 on COCO test-dev split, which has an improvement of 1.7% and 0.8% over the winner of COCO 2017 keypoint Challenge’s single model and their ensembled model [12,10].

Pose tracking follows a similar pipeline of the winner [19] of ICCV’17 PoseTrack Challenge [13]. The single person pose estimation uses our own baseline. The pose tracking (or association) uses the same greedy matching method as in [19]. Our only extension is to use optical flow based pose propagation and similarity measurement. Our best result achieves a mAP score of 74.6 and a MOTA score of 57.8, an absolute 15% and 6% improvement over 59.6 and 51.8 of the winner of ICCV’17 PoseTrack Challenge [19,20]. Our result is the new state-of-the-art on PoseTrack Challenge dataset.

This work is not based on any theoretic evidence. It is based on simple techniques and validated by comprehensive ablation experiments, at our best. Note that we do not claim any algorithmic superiority over previous methods, in spite of better results. We do not perform complete and fair comparison with previous more complex methods, because this is difficult and not our intent. As stated, the contribution of this work are solid baselines for the field.

2 Pose Estimation Using A Deconvolution Head Network

ResNet [18] is the most common backbone network for image feature extraction. It is also used in [15,12] for pose estimation. Our method simply adds a few deconvolutional layers over the last convolution stage in the ResNet, called C_5 . The whole network structure is illustrated in Fig. 1(c). We adopt this structure because it is arguably the simplest to generate heatmaps from deep and low resolution features and also adopted in the state-of-the-art Mask R-CNN [16].

By default, three deconvolutional layers with batch normalization [21] and ReLU activation [22] are used. Each layer has 256 filters with 4×4 kernel. The stride is 2. A 1×1 convolutional layer is added at last to generate predicted heatmaps $\{H_1 \dots H_k\}$ for all k key points.

Same as in [2,4], Mean Squared Error (MSE) is used as the loss between the predicted heatmaps and targeted heatmaps. The targeted heatmap \hat{H}_k for joint k is generated by applying a 2D gaussian centered on the k^{th} joint’s ground truth location.

Discussions To understand the simplicity and rationality of our baseline, we discuss two state-of-the-art network architectures as references, namely, Hourglass [4] and CPN [12]. They are illustrated in Figure 1.

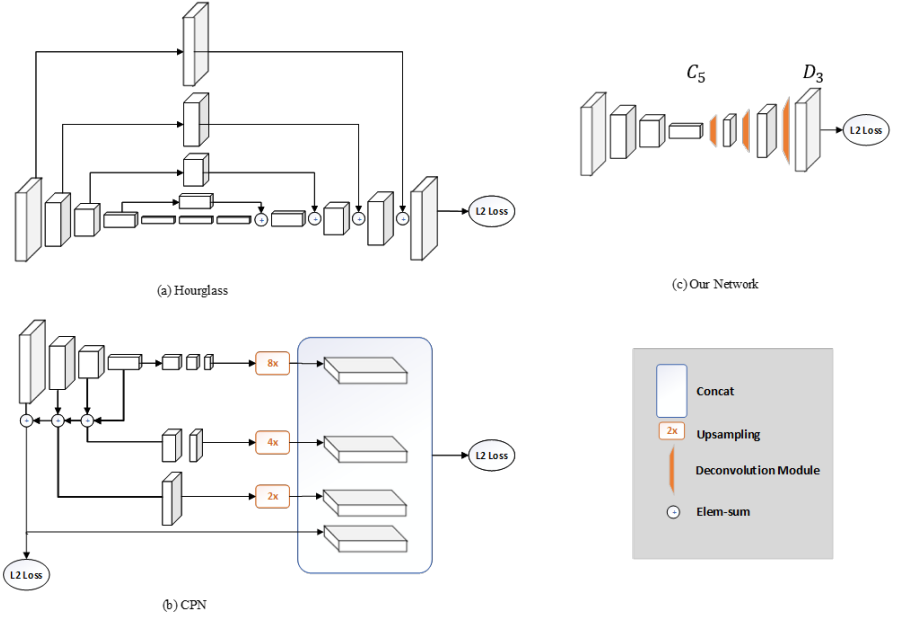


Fig. 1. Illustration of two state-of-the-art network architectures for pose estimation (a) one stage in Hourglass [4], (b) CPN [12], and our simple baseline (c).

Hourglass [4] is the dominant approach on MPII benchmark as it is the basis for all leading methods [5,6,7,8]. It features in a multi-stage architecture with repeated bottom-up, top-down processing and skip layer feature concatenation.

Cascaded pyramid network (CPN) [12] is the leading method on COCO 2017 keypoint challenge [10]. It also involves skip layer feature concatenation and an online hard keypoint mining step.

Comparing the three architectures in Figure 1, it is clear that our method differs from [4,12] in *how high resolution feature maps are generated*. Both works [4,12] use upsampling to increase the feature map resolution and put convolutional parameters in other blocks. In contrary, our method combines the upsampling and convolutional parameters into deconvolutional layers in a much simpler way, without using skip layer connections.

A commonality of the three methods is that three upsampling steps and also three levels of non-linearity (from the deepest feature) are used to obtain high-resolution feature maps and heatmaps. Based on above observations and the good performance of our baseline, it seems that *obtaining high resolution feature maps is crucial, but no matter how*. Note that this discussion is only preliminary and heuristic. It is hard to conclude which architecture in Figure 1 is better, which is not the intent of this work.

3 Pose Tracking Based on Optical Flow

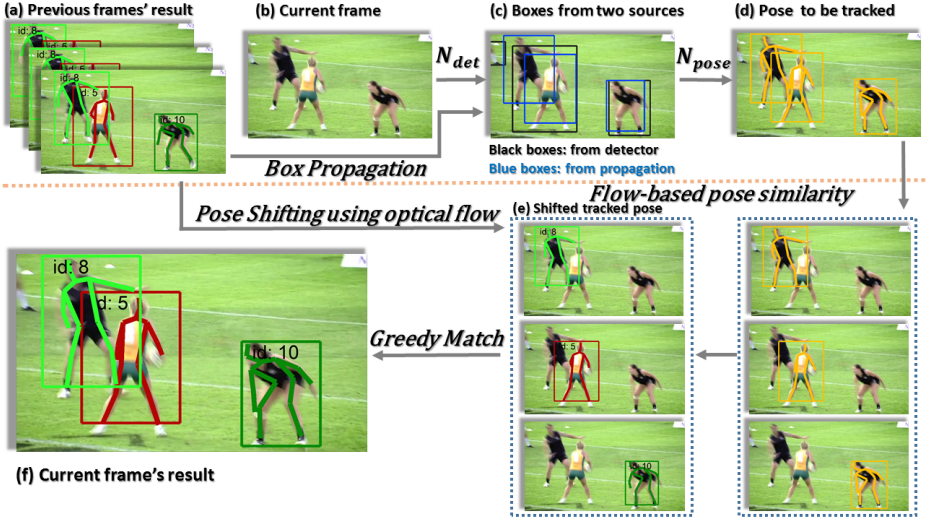


Fig. 2. The proposed flow-based pose tracking framework.

Multi-person pose tracking in videos first needs pose estimation in frames, then tracking human pose by assigning a unique identification (id) number across frames. When processing the k^{th} frame I_k , we have the already processed human instances set $P_{k-1} = \{p_i\}$, $p_i = (joints_i, id_i)$ in frame I_{k-1} which have id to indicate tracks, and the instances set $P_k = \{p_j\}$, $p_j = (joints_j, id_j = None)$ in frame I_k whose id is to be assigned, $joints$ is the set of coordinates of body joints location in images. If p_j is linked to one p_i , then id_i is propagated to id_j , otherwise a new id is assigned to p_j , indicating a new track.

The winner [19] of ICCV'17 PoseTrack Challenge [13] solves this multi-person pose tracking problem by first estimating human pose in frames using Mask R-CNN [16], then performing online tracking using a greedy bipartite matching algorithm frame by frame. The greedy matching algorithm is to first assign the id of p_i in frame I_{k-1} to p_j in frame I_k if the similarity between p_i and p_j is the highest, then remove these two instances from consideration, and repeat the id assigning process with the highest similarity. When an instance p_j in frame I_k has no existing p_i left to link, a new id number is assigned, which indicates a new instance comes up.

We mainly follow this pipeline in [19] with two differences. One is that we have two different kinds of sources for human boxes, from a human detector and propagated from previous frames using optical flow. The second difference is in the similarity metric used by the greedy matching algorithm, we propose to use a flow-based pose similarity metric. Combined with these two modifications, we

have our enhanced flow-based pose tracking algorithm, illustrated in Figure 2. We elaborate the propagation of boxes and the pose similarity metric based on optical flow, then the flow-based pose tracking algorithm in details in the following.

3.1 Box Propagation using Optical Flow

Simply applying a detector designed for single image level (e.g. R-FCN [23]) to videos could lead to missing detections and false detections due to motion blur and occlusion introduced by video frames. As shown in Figure 2(c), the detector misses the left black person due to fast motion. Temporal information is often leveraged to generate more robust detections.

We propose to get boxes for the processing frame from nearby frames using temporal information expressed in optical flow. Given a human instance $p_i = (joints_i, id_i)$ in frame I_{k-1} and the optical flow between frame I_{k-1} and I_k , we could estimate the corresponding $\hat{p}_j = (joints_j, id_j)$ in frame I_k by shifting the joints coordinates of p_i according to the optical flow. Then we compute a bounding box by taking the min and max extents of the shifted $joints_j$, and expand that box by some extend (15% in experiments) as the propagated box.

When the processing frame is difficult for human detectors that could lead to missing detections due to motion blur or occlusion, we could have boxes propagated from previous frames where people have been detected correctly. As shown in Figure 2(c), for the left black person in images, since we have the tracked result in previous frames in Figure 2(a), the propagated boxes successfully contain this person.

3.2 Flow-based Pose Similarity

Using bounding box IoU as the similarity metric (S_{Bbox}) to link instances could be problematic when an instance moves fast thus the boxes do not overlap, and in crowd scenes where boxes may not have the corresponding relationship with instances. A more fine-grained metric could be a pose similarity (S_{Pose}) which calculates the body joints distance between two instances using Object Keypoint Similarity (OKS). The pose similarity could be problematic when the pose of the same person is different across frames due to pose changing. We propose to use a flow-based pose similarity metric.

We have the shifted \hat{p}_i for p_i from frame I_k to I_l by shifting the body joints coordinates using optical flow between frame I_k and I_l . \hat{p}_i roughly represents what the instance p_i from frame I_k should be like in frame I_l . In other words, we could use the similarity of p_j in frame I_l and the shifted \hat{p}_i from I_k to I_l as an agent of the similarity of p_j and p_i to be the same person. This leads to our flow-based pose similarity metric. Given a set of instances $P_k = \{p_i\}$ in frame I_k and a set of instances $P_l = \{p_j\}$ in frame I_l , the flow-based pose similarity metric is represented as

$$S_{Flow}(P_k, P_l) = OKS(\hat{P}_k, P_l), \quad (1)$$

where OKS represents calculating the Object Keypoint Similarity (OKS) between two human pose, and \hat{P}_k represents the shifted instances for P_k from frame I_k to I_l using optical flow from frame I_k to I_l .

Due to occlusions with other people or objects, people often disappear and re-appear again. Considering consecutive two frames is not enough, thus we have the flow-based pose similarity considering multi frames (Multi- S_{flow}), meaning the shifted \hat{P}_k comes from multi previous frames. In this way, we could relink instances even them disappear in middle frames.

3.3 The Flow-based Pose Tracking Algorithm

With the box propagation using optical flow and the flow-based pose similarity, we propose the flow-based pose tracking algorithm combining these two, which is shown in Algorithm 1.

First, we solve the pose estimation problem. For the processing frame in videos, the boxes from a human detector and boxes propagated from previous frames using optical flow is unified using a bounding box Non-Maximum Suppression (NMS) operation. The propagated boxes serve as the complement of missing detections of the detector (e.g. in Figure 2(c)). Then we estimate human pose using the cropped and resized images by these boxes through a pose estimation network.

Second, we solve the tracking problem. We store the tracked instances in a memory pool P_{pool} , which could be used to capture multi frames' linking relationship, initialized in the first frame in a video. For the i^{th} frame I_i , we calculate the flow-based pose similarity matrix Sim between the untracked P_i (id is none) and P_{pool} . Then we assign id to P_i using greedy matching and Sim . Finally we update our tracked instances pool P_{pool} by adding up new instances result P_i . The P_{pool} is realized in a double-ended queue (Deque) with fix capacity manner storing fixed-length frames' instances and the length $pool_{len}$ indicates how many previous frames considered when performing matching.

Algorithm 1 The flow-based inference algorithm for video human pose tracking

- 1: **input:** video frames $\{I_i\}$, instance pool capacity $pool_{len}$.
 - 2: $B_0^{det} = \mathcal{N}_{det}(I_0)$
 - 3: $P_0 = \mathcal{N}_{pose}(I_0, B_0^{det})$
 - 4: $P_{pool} = Deque\{P_0, len = pool_{len}\} \triangleright$ initialize the instance pool with fixed capacity
 - 5: **for** $i = 1$ **to** ∞ **do**
 - 6: $B_i^{det} = \mathcal{N}_{det}(I_i)$
 - 7: B_i^{flow} propagated from I_{i-1} using $F_{i-1 \rightarrow i}$ \triangleright box propagation
 - 8: $B_i = NMS(B_{det}, B_{flow})$ \triangleright unify detection boxes and flow boxes
 - 9: $P_i = \mathcal{N}_{pose}(I_i, B_i)$ \triangleright single image pose estimation
 - 10: $Sim = S_{Flow}(P_{pool}, P_i)$ \triangleright calculate flow-based pose similarity
 - 11: assign track id to P_i using greedy matching, P_{pool} and Sim
 - 12: append P_i to P_{pool} \triangleright update the instance pool
 - 13: **end for**
-

4 Experiments

4.1 Pose Estimation on COCO.

The COCO Keypoint Challenge [9] requires localization of multi-person keypoints in challenging uncontrolled conditions. The COCO train, validation, and test sets contain more than 200k images and 250k person instances labeled with keypoints. 150k instances of them are publicly available for training and validation. Our models are only trained on all COCO *train2017* dataset (includes 57K images and 150K person instances) no extra data involved, ablation are studied on the *val2017* set and finally we report the final results on *test-dev2017* set to make a fair comparison with the public state-of-the-art results [11,16,15,12].

The COCO evaluation defines the object keypoint similarity (OKS) and uses the mean average precision (AP) over 10 OKS thresholds as main competition metric [10]. The OKS plays the same role as the IoU in object detection. It is calculated from the distance between predicted points and ground truth points normalized by scale of the person.

Training. The ground truth human box is made to a fixed aspect ratio, e.g., *height : width* = 4 : 3 by extending the box in height or width. It is then cropped from the image and resized to a fixed resolution. The default resolution is 256 : 192. It is the same as the state-of-the-art method [12] for a fair comparison. Data augmentation includes scale($\pm 30\%$), rotation(± 40 degrees) and flip.

Our ResNet [18] backbone network is initialized by pre-training on ImageNet classification task [24]. In the training for pose estimation, the base learning rate is $1e-3$. It drops to $1e-4$ at 90 epochs and $1e-5$ at 120 epochs. There are 140 epochs in total. Mini-batch size is 128. Adam [25] optimizer is used. Four GPUs on a GPU server is used. MxNet [26] is used for implementation.

ResNet of depth 50, 101 and 152 layers are experimented. ResNet-50 is used by default, unless otherwise noted.

Testing. A two-stage top-down paradigm is applied, similar as in [15,12]. For detection, by default we use a faster-RCNN [27] detector with detection AP 56.4 for the person category on COCO *val2017*. Following the common practice in [12,4], the joint location is predicted on the averaged heatmaps of the original and flipped image. A quarter offset in the direction from highest response to the second highest response is used to obtain the final location. Fig. 3 has shown some sample results using our ResNet-152 model.

Ablation Study. Table 1 investigates various options in our baseline in Section 2.

1. *Heat map resolution.* Method (a) uses three deconvolutional layers to generate 64×48 heatmaps. Method (b) generates 32×24 heatmaps with two deconvolutional layers. (a) outperform (b) by 2.4 AP with only slightly increased model capacity. By default, three deconvolutional layers are used.

Table 1. Ablation study of our baseline method on COCO val2017 dataset. Those setting used in comparison are **bolded**. For example, (a, e, f) compares backbones.

Method	Backbone	Input Size	#Deconv. Layers	Deconv. Kernel Size	AP
<i>a</i>	ResNet-50	256×192	3	4	70.6
<i>b</i>	ResNet-50	256×192	2	4	68.2
<i>c</i>	ResNet-50	256×192	3	2	70.3
<i>d</i>	ResNet-50	256×192	3	3	70.4
<i>e</i>	ResNet-101	256×192	3	4	71.7
<i>f</i>	ResNet-152	256×192	3	4	72.4
<i>g</i>	ResNet-50	128×96	3	4	60.6
<i>h</i>	ResNet-50	384×288	3	4	72.2

Table 2. Comparison with Hourglass [4] and CPN [12] on COCO val2017 dataset. Their results are cited from [12]. OHKM means Online Hard Keypoints Mining.

Method	Backbone	Input Size	OHKM	AP
8-stage Hourglass	-	256×192	✗	66.9
8-stage Hourglass	-	256×256	✗	67.1
CPN	ResNet-50	256×192	✗	68.6
CPN	ResNet-50	384×288	✗	70.6
CPN	ResNet-50	256×192	✓	69.4
CPN	ResNet-50	384×288	✓	71.6
Ours	ResNet-50	256×192	✗	70.6
Ours	ResNet-50	384×288	✗	72.2

2. *Kernel size.* Methods (a, c, d) show that a smaller kernel size gives a marginally decrease in AP, which is 0.3 point decrease from kernel size 4 to 2. By default, deconvolution kernel size of 4 is used.
3. *Backbone.* As in most vision tasks, a deeper backbone model has better performance. Methods (a, e, f) show steady improvement by using deeper backbone models. AP increase is 1.1 from ResNet-50 to Resnet-101 and 1.8 from ResNet-50 to ResNet-152.
4. *Image size.* Methods (a, g, h) show that image size is critical for performance. From method (a) to (g), the image size is reduced by half and AP drops points. On the other hand, relative 75% computation is saved. Method (h) uses a large image size and increases 1.6 AP from method (a), at the cost of higher computational cost.

Comparison with Other Methods on COCO val2017 Table 2 compares our results with a 8-stage Hourglass [4] and CPN [12]. All the three methods use a similar top-down two-stage paradigm. For reference, the person detection AP of hourglass [4] and CPN [12] is 55.3 [12], which is comparable to ours 56.4.

Table 3. Comparisons on COCO test-dev dataset. **Top:** methods in the literature, trained only on COCO training dataset. **Middle:** results submitted to COCO test-dev leaderboard [10], which have either extra training data (*) or models ensembled (+). **Bottom:** our single model results, trained only on COCO training dataset.

Method	Backbone	Input Size	AP	AP ₅₀	AP ₇₅	AP _m	AP _l	AR
CMU-Pose [11]	-	-	61.8	84.9	67.5	57.1	68.2	66.5
Mask-RCNN [16]	ResNet-50-FPN	-	63.1	87.3	68.7	57.8	71.4	-
G-RMI [15]	ResNet-101	353 × 257	64.9	85.5	71.3	62.3	70.0	69.7
CPN [12]	ResNet-Inception	384 × 288	72.1	91.4	80.0	68.7	77.2	78.5
FAIR Mask R-CNN* [10]	ResNeXt-101-FPN	-	69.2	90.4	77.0	64.9	76.3	75.2
G-RMI* [10]	ResNet-152	353 × 257	71.0	87.9	77.7	69.0	75.2	75.8
oks* [10]	-	-	72.0	90.3	79.7	67.6	78.4	77.1
bangbangren*+ [10]	ResNet-101	-	72.8	89.4	79.6	68.6	80.0	78.7
CPN+ [12,10]	ResNet-Inception	384 × 288	73.0	91.7	80.9	69.5	78.1	79.0
Ours	ResNet-50	256 × 192	70.2	90.9	78.3	67.1	75.9	75.8
Ours	ResNet-50	384 × 288	71.3	91.0	78.5	67.3	77.9	76.6
Ours	ResNet-101	256 × 192	71.1	91.1	79.3	68.3	76.7	76.8
Ours	ResNet-101	384 × 288	73.2	91.4	80.9	69.7	79.5	78.6
Ours	ResNet-152	256 × 192	71.9	91.4	80.1	68.9	77.4	77.5
Ours	ResNet-152	384 × 288	73.8	91.7	81.2	70.3	80.0	79.1

Compared with Hourglass [4,12], our baseline has an improvement of 3.7 in AP. Both methods use an input size of 256×192 and no Online Hard Keypoints Mining(OHKM) involved.

CPN [12] and our baseline use the same backbone of ResNet-50. When OHKM is not used, our baseline outperforms CPN [12] by 2.0 AP for input size 256×192 , and 1.6 AP for input size 384×288 . When OHKM is used in CPN [12], our baseline is better by 0.6 AP for both input sizes.

Note that the results of Hourglass [4] and CPN [12] are cited from [12] and not implemented by us. Therefore, the performance difference could come from implementation difference. Nevertheless, we believe it is safe to conclude that our baseline has comparable results but is simpler.

Comparisons on COCO test-dev dataset Table 3 summarizes the results of other state-of-the-art methods in the literature on COCO Keypoint Leaderboard [10] and COCO *test-dev* dataset. For our baseline here, a human detector with *person detection* AP of 60.9 on COCO *std-dev* split dataset is used. For reference, CPN [12] use a human detector with *person detection* AP of 62.9 on COCO *minival* split dataset.

Compared with CMU-Pose [11], which is a bottom-up approach for multi-person pose estimation, our method is significantly better. Both G-RMI [15] and CPN [12] have a similar top-down pipeline with ours. G-RMI also uses ResNet as backbone, as ours. Using the same backbone Resnet-101, our method outperforms G-RMI for both small (256×192) and large input size (384×288). CPN uses a stronger backbone of ResNet-Inception [28]. As evidence, the top-1 error rate on ImageNet validation set of Resnet-Inception and ResNet-152 are 18.7% and 21.4% respectively [28]. Yet, for the same input size 384×288 , our result 73.8 outperforms both CPN’s single model and their ensembled model, which have 72.1 and 73.0 respectively.

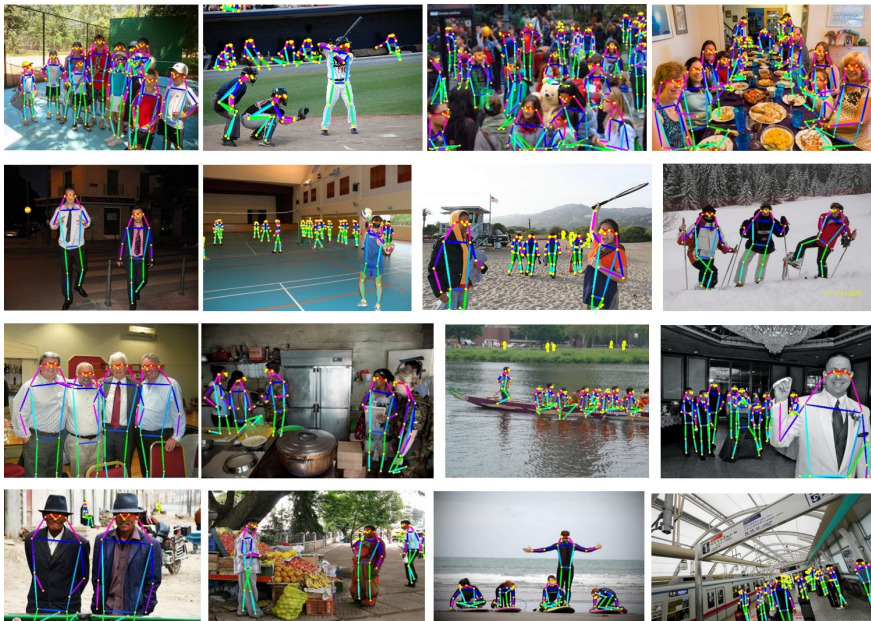


Fig. 3. Some sample results on COCO.

4.2 Pose Estimation and Tracking on PoseTrack

PoseTrack [13] dataset is a large-scale benchmark for multi-person pose estimation and tracking in videos. It requires not only pose estimation in single frames, but also temporal tracking across frames. It contains 514 videos including 66,374 frames in total, split into 300, 50 and 208 videos for training, validation and test set respectively. For training videos, 30 frames from the center are annotated. For validation and test videos, besides 30 frames from the center, every fourth frame is also annotated for evaluating long range articulated tracking. The annotations include 15 body keypoints location, a unique person id and a head bounding box for each person instance.

The dataset has three tasks. Task 1 evaluates single-frame pose estimation using mean average precision (mAP) metric as is done in [29]. Task 2 also evaluates pose estimation but allows usage of temporal information across frames. Task 3 evaluates tracking using multi-object tracking metrics [30]. As our tracking baseline uses temporal information, we report results on Task 2 and 3. Note that our pose estimation baseline also performs best on Task 1 but is not reported here for simplicity.

Training Our pose estimation model is fine-tuned from those pre-trained on COCO in Section 4.1. As only key points are annotated, we obtain the ground

truth box of a person instance by extending the bounding box of its all key points by 15% in length (7.5% on both sides). The same data augmentation as in Section 4.1 is used. During training, the base learning rate is $1e-4$. It drops to $1e-5$ at 10 epochs and $1e-6$ at 15 epochs. There are 20 epochs in total. Other hyper parameters are the same as in Section 4.1.

Testing Our flow based tracking baseline is closely related to the human detector’s performance, as the propagated boxes could affect boxes from a detector. To investigate its effect, we experiment with two off-the-shelf detectors, a faster but less accurate R-FCN [23] and a slower but more accurate FPN-DCN [31]. Both uses ResNet-101 backbone and are obtained from public implementation [32]. No additional fine tuning of detectors on PoseTrack dataset is performed.

Similar as in [19], we first drop low-confidence detections, which tends to decrease the mAP metric but increase the MOTA tracking metric. Also, since the tracking metric MOT penalizes false positives equally regardless of the scores, we drop low confidence joints first to generate the result as in [19]. We choose the boxes and joints drop threshold in a data-driven manner on validation set, 0.5 and 0.4 respectively.

Fig. 4 illustrates some results of our approach on PoseTrack test dataset.



Fig. 4. Some sample results on PoseTrack Challenge test set.

Table 4. Ablation study on PoseTrack Challenge validation dataset. **Top:** Results of ResNet-50 backbone using R-FCN detector. **Middle:** Results of ResNet-50 backbone using FPN-DCN detector. **Bottom:** Results of ResNet-152 backbone using FPN-DCN detector.

Method	Backbone	Detector	With Box Propagation	Similarity Metric	mAP Total	MOTA Total	MOTP Total	Prec Total	Rec Total
a_1	ResNet-50	R-FCN	\times	S_{Bbox}	66.0	57.6	84.8	89.3	68.9
a_2	ResNet-50	R-FCN	\times	S_{Pose}	66.0	57.7	84.8	89.3	68.9
a_3	ResNet-50	R-FCN	\checkmark	S_{Bbox}	70.3	61.4	84.6	88.0	73.5
a_4	ResNet-50	R-FCN	\checkmark	S_{Pose}	70.3	61.8	84.6	88.0	73.6
a_5	ResNet-50	R-FCN	\checkmark	S_{Flow}	70.3	61.8	84.6	88.0	73.5
a_6	ResNet-50	R-FCN	\checkmark	Multi- S_{Flow}	70.3	62.2	84.6	88.0	73.5
b_1	ResNet-50	FPN-DCN	\times	S_{Bbox}	69.3	59.8	84.6	87.4	72.7
b_2	ResNet-50	FPN-DCN	\times	S_{Pose}	69.3	59.7	84.6	87.4	72.7
b_3	ResNet-50	FPN-DCN	\checkmark	S_{Bbox}	72.4	62.1	84.5	86.3	76.0
b_4	ResNet-50	FPN-DCN	\checkmark	S_{Pose}	72.4	61.8	84.5	86.3	76.0
b_5	ResNet-50	FPN-DCN	\checkmark	S_{Flow}	72.4	62.4	84.5	86.3	76.0
b_6	ResNet-50	FPN-DCN	\checkmark	Multi- S_{Flow}	72.4	62.9	84.5	86.3	76.0
c_1	ResNet-152	FPN-DCN	\times	S_{Bbox}	72.9	62.0	85.5	86.9	76.2
c_2	ResNet-152	FPN-DCN	\times	S_{Pose}	72.9	61.9	85.5	86.9	76.2
c_3	ResNet-152	FPN-DCN	\checkmark	S_{Bbox}	76.7	64.8	85.4	85.5	80.3
c_4	ResNet-152	FPN-DCN	\checkmark	S_{Pose}	76.7	64.9	85.4	85.5	80.3
c_5	ResNet-152	FPN-DCN	\checkmark	S_{Flow}	76.7	65.1	85.4	85.5	80.3
c_6	ResNet-152	FPN-DCN	\checkmark	Multi- S_{Flow}	76.7	65.4	85.4	85.5	80.3

Table 5. Multi-person Pose Estimation Performance on PoseTrack Challenge dataset. “*” means models trained on train+validation set. **Top:** Results on PoseTrack validation set. **Bottom:** Results on PoseTrack test set

Method	Dataset	Head mAP	Shoulder mAP	Elbow mAP	Wrist mAP	Hip mAP	Knee mAP	Ankle mAP	Total mAP
Girdhar et al. [19]	validation	67.5	70.2	62.0	51.7	60.7	58.7	49.8	60.6
Xiu et al. [35]	validation	66.7	73.3	68.3	61.1	67.5	67.0	61.3	66.5
Ours:ResNet-50	validation	79.1	80.5	75.5	66.0	70.8	70.0	61.7	72.4
Ours:ResNet-152	validation	81.7	83.4	80.0	72.4	75.3	74.8	67.1	76.7
Girdhar et al.* [19]	test	-	-	-	-	-	-	-	59.6
Xiu et al. [35]	test	64.9	67.5	65.0	59.0	62.5	62.8	57.9	63.0
Ours:ResNet-50	test	76.4	77.2	72.2	65.1	68.5	66.9	60.3	70.0
Ours:ResNet-152	test	79.5	79.7	76.4	70.7	71.6	71.3	64.9	73.9
Ours:ResNet-152*	test	80.1	80.1	76.9	71.5	72.5	72.4	65.7	74.6

For optical flow estimation, the fastest model FlowNet2S in FlowNet family [33] is used, as provided on [34]. We use the PoseTrack evaluation toolkit for results on validation set and report final results on test set from the evaluation server.

Our main ablation study is performed on ResNet-50 with input size 256×192 , which is already strong when compared with state-of-the-art. Our best result is on ResNet-152 with input size 384×288 .

Effect of Box Propagation Table 4 shows that box propagation introduces improvement on both mAP and MOTA metrics using different backbones and detectors. With R-FCN detector, using box propagation (method a_3 vs. a_1) introduces improvement of 4.3 % mAP and 3.8 % MOTA. With the better FPN-DCN detector, using box propagation (method b_3 vs. b_1) introduces improvement of 3.1 %mAP and 2.3 % MOTA. With ResNet-152 as backbone (method c_3 vs. c_1), improvement is 3.8 % mAP and 2.8 % MOTA. Note that such improvement

Table 6. Multi-person Pose Tracking Performance on PoseTrack Challenge dataset. “*” means models trained on train+validation set. **Top:** Results on PoseTrack validation set. **Bottom:** Results on PoseTrack test set

Method	Dataset	MOTA Head	MOTA Shou	MOTA Elb	MOTA Wri	MOTA Hip	MOTA Knee	MOTA Ank	MOTA Total	MOTP Total	Prec Total	Rec Total
Girdhar et al. [19]	validation	61.7	65.5	57.3	45.7	54.3	53.1	45.7	55.2	61.5	66.4	88.1
Xiu et al. [35]	validation	59.8	67.0	59.8	51.6	60.0	58.4	50.5	58.3	67.8	70.3	87.0
Ours:ResNet-50	validation	72.1	74.0	61.2	53.4	62.4	61.6	50.7	62.9	84.5	86.3	76.0
Ours:ResNet-152	validation	73.9	75.9	63.7	56.1	65.5	65.1	53.5	65.4	85.4	85.5	80.3
Girdhar et al.* [19]	test	-	-	-	-	-	-	-	51.8	-	-	-
Xiu et al. [35]	test	52.0	57.4	52.8	46.6	51.0	51.2	45.3	51.0	16.9	71.2	78.9
Ours:ResNet-50	test	65.9	67.0	51.5	48.0	56.2	54.6	46.9	56.4	45.5	81.0	75.7
Ours:ResNet-152	test	67.1	68.4	52.2	48.9	56.1	56.6	48.8	57.6	62.6	79.4	79.9
Ours:ResNet-152*	test	67.3	68.5	52.3	49.3	56.8	57.2	48.6	57.8	57.3	79.4	80.3

does not only come from more boxes. As noted in [19], simply keeping more boxes of a detector, e.g., by using a smaller threshold, would lead to an improvement in mAP, but a drop in MOTA since more false positives would be introduced. The box propagation improves both mAP and MOTA metrics, indicating that it finds more persons that are missed by the detector, possibly due to motion blur or occlusion in video frames.

Another interesting observation is that the less accurate R-FCN detector benefits more from box propagation. For example, the gap between using FPN-DCN and R-FCN detector in ResNet-50 is decreased from 3.3% mAP and 2.2% MOTA (from a_1 to b_1) to 2.1% mAP and 0.4% MOTA (from a_3 to b_3). Also, method a_3 outperforms method b_1 by 1.0% mAP and 1.6% MOTA, indicating that a weak detector R-FCN combined with box propagation could perform better than a strong detector FPN-DCN along. While, the former is more efficient as box propagation is fast.

Effect of Flow-based Pose Similarity Flow-based pose similarity is shown working better when compared with bounding box similarity and pose similarity in Table 4. For example, flow-based similarity using multi frames (method b_6) and single frame (method b_5) outperforms bounding box similarity (method b_3) by 0.8% MOTA and 0.3% MOTA.

Note that flow-based pose similarity is better than bounding box similarity when person moves fast and their boxes do not overlap. Method b_6 with flow-based pose similarity considers multi frames and have an 0.5% MOTA improvement when compared to method b_5 , which considers only one previous frame. This improvement comes from the case when people are lost shortly due to occlusion and appear again.

Comparison with State-of-the-Art We report our results on both Task 2 and Task 3 on PoseTrack dataset. As verified in Table 4, method b_6 and c_6 are the best settings and used here. Backbones are ResNet-50 and ResNet-152, respectively. The detector is FPN-DCN [31].

Table 7. Results of Mulit-Person Pose Tracking on PoseTrack Challenge Leaderboard. “*” means models trained on train+validation set.

Entry	Pose Model	Tracking Model	Additional Training Dataset	mAP	MOTA
ProTracker [19]	Mask R-CNN* [16]	Hungarian	COCO	59.6	51.8
PoseFlow [20]	-	-	COCO+MPII-Pose	63.0	51.0
MVIG [20]	-	-	COCO+MPII-Pose	63.2	50.7
BUTD2 [36]	PAF [11]	graph partitioning	COCO	59.2	50.6
SOPT-PT [20]	-	-	COCO+MPII-Pose	58.2	42.0
ML-LAB [37]	modification of PAF [11]	frame-to-frame assign	COCO+MPII-Pose	70.3	41.8
Ours	ResNet152*	Greedy Match	COCO	74.6	57.8

Table 5 reports the results on pose estimation (Task 2). Our small model (ResNet-50) outperforms the other methods already by a large margin. Our larger model (ResNet-152) further improves the state-of-the-art. It has an absolute 15% improvement in mAP over [19], which is the winner of ICCV’17 PoseTrack Challenge, and also has an 11.6% improvement over a recent work [35], which is the previous best.

Table 6 reports the results on pose tracking (Task 3). Compared with [19] on validation dataset on PoseTrack, our best model (ResNet-152) has an 10.2 improvement in MOTA over its 55.2. On test dataset, there also has an improvement of 6%. Compared with the recent work [35], our best model (ResNet-152*) has 7.1% and 6.8% improvement on validation and test dataset, respectively. Note that our smaller model (ResNet-50) also outperform the other methods [19,35].

Table 7 summarizes the results on PoseTrack’s leaderboard. Our baseline outperforms all public entries by a large margin. Note that all methods differ significantly and this comparison is only on system level.

5 Conclusions

We present simple and strong baselines for pose estimation and tracking. They achieve state-of-the-art results on challenging benchmarks. They are validated via comprehensive ablation studies. We hope such baselines would benefit the field by easing the idea development and evaluation.

References

1. Toshev, A., Szegedy, C.: Deeppose: Human pose estimation via deep neural networks. In: Proceedings of the IEEE Conference on Computer Vision and Pattern Recognition. (2014) 1653–1660
2. Tompson, J.J., Jain, A., LeCun, Y., Bregler, C.: Joint training of a convolutional network and a graphical model for human pose estimation. In: Advances in neural information processing systems. (2014) 1799–1807
3. Andriluka, M., Pishchulin, L., Gehler, P., Schiele, B.
4. Newell, A., Yang, K., Deng, J.: Stacked hourglass networks for human pose estimation. In: European Conference on Computer Vision, Springer (2016) 483–499

5. Chu, X., Yang, W., Ouyang, W., Ma, C., Yuille, A.L., Wang, X.: Multi-context attention for human pose estimation. arXiv preprint arXiv:1702.07432 (2017)
6. Chou, C.J., Chien, J.T., Chen, H.T.: Self adversarial training for human pose estimation. arXiv preprint arXiv:1707.02439 (2017)
7. Chen, Y., Shen, C., Wei, X.S., Liu, L., Yang, J.: Adversarial posenet: A structure-aware convolutional network for human pose estimation. In: IEEE International Conference on Computer Vision. (2017) 1212–1221
8. Yang, W., Li, S., Ouyang, W., Li, H., Wang, X.: Learning feature pyramids for human pose estimation. In: IEEE International Conference on Computer Vision. (2017)
9. Lin, T.Y., Maire, M., Belongie, S., Hays, J., Perona, P., Ramanan, D., Dollár, P., Zitnick, C.L.: Microsoft coco: Common objects in context. In: European conference on computer vision, Springer (2014) 740–755
10. COCO: COCO Leader Board. <http://cocodataset.org>
11. Cao, Z., Simon, T., Wei, S.E., Sheikh, Y.: Realtime multi-person 2d pose estimation using part affinity fields. In: CVPR. (2017)
12. Chen, Y., Wang, Z., Peng, Y., Zhang, Z., Yu, G., Sun, J.: Cascaded pyramid network for multi-person pose estimation. arXiv preprint arXiv:1711.07319 (2017)
13. Iqbal, U., Milan, A., Andriluka, M., Ensafutdinov, E., Pishchulin, L., Gall, J., Schiele, B.: PoseTrack: A benchmark for human pose estimation and tracking. arXiv:1710.10000 [cs] (2017)
14. Newell, A., Huang, Z., Deng, J.: Associative embedding: End-to-end learning for joint detection and grouping. In: Advances in Neural Information Processing Systems. (2017) 2274–2284
15. Papandreou, G., Zhu, T., Kanazawa, N., Toshev, A., Tompson, J., Bregler, C., Murphy, K.: Towards accurate multiperson pose estimation in the wild. arXiv preprint arXiv:1701.01779 8 (2017)
16. He, K., Gkioxari, G., Dollár, P., Girshick, R.: Mask r-cnn. In: Computer Vision (ICCV), 2017 IEEE International Conference on, IEEE (2017) 2980–2988
17. Andriluka, M., Iqbal, U., Milan, A., Insafutdinov, E., Pishchulin, L., Gall, J., Schiele, B.: Posetrack: A benchmark for human pose estimation and tracking. arXiv preprint arXiv:1710.10000 (2017)
18. He, K., Zhang, X., Ren, S., Sun, J.: Deep residual learning for image recognition. In: Proceedings of the IEEE conference on computer vision and pattern recognition. (2016) 770–778
19. Girdhar, R., Gkioxari, G., Torresani, L., Paluri, M., Tran, D.: Detect-and-track: Efficient pose estimation in videos. arXiv preprint arXiv:1712.09184 (2017)
20. PoseTrack: PoseTrack Leader Board. <https://posetrack.net/leaderboard.php>
21. Ioffe, S., Szegedy, C.: Batch normalization: Accelerating deep network training by reducing internal covariate shift. In: International conference on machine learning. (2015) 448–456
22. Krizhevsky, A., Sutskever, I., Hinton, G.E.: Imagenet classification with deep convolutional neural networks. In: Advances in neural information processing systems. (2012) 1097–1105
23. Jifeng Dai, Yi Li, K.H., Sun, J.: R-FCN: Object detection via region-based fully convolutional networks. (2016)
24. Russakovsky, O., Deng, J., Su, H., Krause, J., Satheesh, S., Ma, S., Huang, Z., Karpathy, A., Khosla, A., Bernstein, M., et al.: Imagenet large scale visual recognition challenge. International Journal of Computer Vision **115**(3) (2015) 211–252
25. Kingma, D.P., Ba, J.: Adam: A method for stochastic optimization. arXiv preprint arXiv:1412.6980 (2014)

26. Chen, T., Li, M., Li, Y., Lin, M., Wang, N., Wang, M., Xiao, T., Xu, B., Zhang, C., Zhang, Z.: Mxnet: A flexible and efficient machine learning library for heterogeneous distributed systems. arXiv preprint arXiv:1512.01274 (2015)
27. Ren, S., He, K., Girshick, R., Sun, J.: Faster r-cnn: Towards real-time object detection with region proposal networks. In: Advances in neural information processing systems. (2015) 91–99
28. Szegedy, C., Ioffe, S., Vanhoucke, V., Alemi, A.A.: Inception-v4, inception-resnet and the impact of residual connections on learning. In: AAAI. Volume 4. (2017) 12
29. Pishchulin, L., Insafutdinov, E., Tang, S., Andres, B., Andriluka, M., Gehler, P.V., Schiele, B.: Deepcut: Joint subset partition and labeling for multi person pose estimation. In: Proceedings of the IEEE Conference on Computer Vision and Pattern Recognition. (2016) 4929–4937
30. Bernardin, K., Stiefelhagen, R.: Evaluating multiple object tracking performance: the clear mot metrics. Journal on Image and Video Processing **2008** (2008) 1
31. Jifeng Dai, Haozhi Qi, Y.X.Y.L.G.Z.H.H., Wei, Y.: Deformable convolutional networks. arXiv preprint arXiv:1703.06211 (2017)
32. : Deformable-ConvNet. <https://github.com/msracver/Deformable-ConvNets>
33. Ilg, E., Mayer, N., Saikia, T., Keuper, M., Dosovitskiy, A., Brox, T.: FlowNet 2.0: Evolution of optical flow estimation with deep networks. In: IEEE Conference on Computer Vision and Pattern Recognition (CVPR). Volume 2. (2017)
34. NVIDIA: flownet2-pytorch. <https://github.com/NVIDIA/flownet2-pytorch> (2018) [Online; accessed March-2018].
35. Xiu, Y., Li, J., Wang, H., Fang, Y., Lu, C.: Pose flow: Efficient online pose tracking. arXiv preprint arXiv:1802.00977 (2018)
36. Jin, S., Ma, X., Han, Z., Wu, Y., Yang, W., Liu, W., Qian, C., Ouyang, W.: Towards multi-person pose tracking: Bottom-up and top-down methods. In: ICCV PoseTrack Workshop. (2017)
37. Zhu, X., Jiang, Y., Luo, Z.: Multi-person pose estimation for posetrack with enhanced part affinity fields. In: ICCV PoseTrack Workshop. (2017)